Theoretical search for possible Au-Si crystal structures using a genetic algorithm

Yue-Hang Dong,[1,2] Wen-Cai Lu,[1,3,*] Xin Xu,[3] Xin Zhao,[4] K. M. Ho,[4] and C. Z. Wang[4,†]
[1]*Institute of Theoretical Chemistry, Jilin University, Changchun, Jilin 130021, P. R. China*
[2]*School of Data Science and Software Engineering, Qingdao University, Qingdao, Shandong 266071, P. R. China*
[3]*College of Physics and Laboratory of Fiber Materials and Modern Textile, Growing Base for State Key Laboratory, Qingdao University, Qingdao, Shandong 266071, P. R. China*
[4]*Ames Laboratory–U.S. DOE and Department of Physics and Astronomy, Iowa State University, Ames, Iowa 50011, USA*
(Received 29 December 2016; revised manuscript received 27 February 2017; published 18 April 2017)

We performed a global search for possible Au-Si crystal structures using a genetic algorithm (GA) combined with density functional theory (DFT) calculations. Two Au-Si structures, Au_8Si_8 and $Au_{16}Si_8$, were found to be energetically stable and have no imaginary frequencies by phonon calculations. The formation energies of all the studied structures gave a convex hull of the Au-Si system, showing that the most stable composition was Au-Si = 1 : 1 and that the Si-rich structures were much less stable than the Au-rich ones.

DOI: 10.1103/PhysRevB.95.134109

I. INTRODUCTION

Metal-semiconductor interaction is a subject of considerable interest with regard to both technical applications [e.g., metal-insulator-semiconductor (MIS) devices] and fundamental research (e.g., Schottky barrier) [1,2]. The Au-Si system, as a typical example of metal-semiconductor alloy, has drawn considerable attention due to the deep eutectic region in such system. For instance, the melting point decreases to 363 °C for 81.0% Au [3], as compared with melting temperatures 1064 °C and 1414 °C for pure Au and Si, respectively. In semiconductor industry, Au and Si are widely used in soldering and making electrical contacts, which can be used to form a lifetime controller for electric-charge carriers in fast-switching devices and microchip packing and interconnection in microelectromechanical systems (MEMS) [4–7]. Moreover, in nanotechnology, the Au-Si eutectic alloy is also of great interest for growing Si nanowires [8].

While stable bulk crystalline Au-Si intermetallic compounds are hard to form [9,10], the Au-Si alloy was discovered as the first binary metallic glass-forming alloys [11]. By using rapid quenching, a technique that has been known to produce meta-stable phases [12], the Au-Si amorphous alloy can be obtained from liquid Au-Si. Although the Au-Si amorphous alloy exhibits remarkable physical properties, the atomic structure and formation mechanism of amorphous alloys remain poorly understood [10,13,14]. Gold silicide structures at different compositions have also been an interesting subject of research and have attached several investigations. Various experimental methods have been used such as evaporation, irradiation [15,16], sputter deposition, blast-atomizing rapid quenching and x-ray diffraction (XRD) to investigate the formation and structures of possible stable and metastable phases of gold silicide [10,17,18]. It has been reported that Au deposition on a Si substrate can lead to the formation of silicide even at room temperature. Si atoms diffuse from the Si substrate and cross through the Au overlayer to form an Au-Si thin film alloy on the Au surface [19]. Another observation is that a layer of Au_3Si_2 formed at the top of the Au film when Au atoms were deposited on Si(111) at room temperature [20]. The structure of the eutectic liquid was experimentally investigated via XRD measurements in study [18]. By using glancing angle XRD, Shpyrko *et al.* discovered a crystalline monolayer on top of the eutectic liquid of $Au_{82}Si_{18}$ under the temperature higher than the alloy's melting point [10]. However, none of the experimental studies mentioned above provided detailed structure information about the observed alloy phases due to the complexity of Au-Si alloys [10,17,20–22]. Resolving the structures of complex alloys experimentally is still very difficult, which impedes the understanding and further optimization of the alloys for applications [23]. On the other hand, computational algorithms and methods for *ab initio* structure prediction can speed up the investigation of the structures of the Au-Si alloy [24,25]. Pasturel *et al.* investigated the Au-Si system via *ab initio* molecular dynamics (AIMD) simulations [26]; they revealed that Au and Si atoms are very reactive with each other [13,27] and that they lead to strong intermixing between Si and Au atoms [26]. By first-principles electronic structure calculations, Tasci *et al.* predicted a new ground state of crystalline Au_4Si in spite of the fact that no Au-Si compounds have been shown in the existing phase diagram [28]. Lee and Hwanga examined the atomic structures, energetics, and the bonding of amorphous Au-Si alloys [13]. They also studied the surface segregation behavior of Si in amorphous Au-Si alloys using AIMD [27]. Lee and Hwang's results [13] predicted that the stable structure of Au-Si alloys can be formed when the Si content is around 40–50%, with an energy gain of about 0.15 eV/atom.

In this paper, we applied the genetic algorithm (GA) to search for possible stable crystal structures of Au-Si compounds. Our studies predict several new stable Au-Si compounds. The dynamical stability and the electronic properties of these new compounds were also studied by first-principles calculations. The predictions from our theoretical studies would provide useful guidance for experimental synthesis and discovery of new compounds for Au-Si systems.

II. METHOD

Applications of GA to perform the global optimization to search for the stable atomic structures of clusters and crystals

*Corresponding author: wencailu@jlu.edu.cn
†Corresponding author: wangcz@ameslab.gov

have been rapidly developed recently due to the advances of the computer power and computational software. The adaptive GA (AGA) code [30,31] used in this paper is based on real space cut-and-paste operations [29] and has been successfully applied to predictions of many complex crystal structures [23,32], such as the atomic structure of a rare-earth (RE) free permanent magnetic material—Zr_2Co_{11} [23]—and the layered structures of thin film solar cell materials—Cu_2Te and Cu_2Se [32]. In the present paper, we performed a systematic GA search for the Au-Si crystal structure using first-principles calculations as the energy evaluation method. The GA searches were performed without any preassumptions on the type of Bravais lattice, the atom basis, or the unit cell dimensions. The chemical compositions were the only given information, and the initial atomic positions in the unit cells were randomly generated.

Considering that a pure Au conventional cell is a face centered cubic (fcc) structure (No. 225, Fm-$3m$) with four atoms, and a pure Si conventional cell is a diamond structure (No. 227, Fd-$3m$) with eight atoms, our searching therefore started from cells with eight atoms, which is their least common multiple, such as Au_7Si, Au_6Si_2, Au_5Si_3, Au_4Si_4, Au_3Si_5, Au_2Si_6, and $AuSi_7$. We also considered the cells of similar size with a varied number of atoms in the unit cell from seven to 12 to cover some special compositions that were mentioned in the literature, such as Au_4Si [28], Au_2Si [21,42], Au_3Si_2 [20], $AuSi_2$, and Au_4Si_3 [10,21]. The searches were performed for unit cells with 4–6 up to 16–24 atoms, and a population of 32 (64) structures were used for unit cells containing up to 12 (24) atoms. Each GA search was considered to be converged after the lowest energy of the population remains unchanged in 200 steps. The low-energy structures of these 12 compositions were collected from GA searches for finer structure optimization.

The first-principles calculations were performed using density functional theory (DFT) within generalized-gradient approximation (GGA) with projector-augmented wave (PAW) pseudopotential method by Vienna *Ab initio* Simulation Package (VASP) code [33–36]. The GGA exchange-correlation energy functional parameterized by Perdew, Burke, and Ernzerhof (PBE) was used [37]. The kinetic energy cutoff for the plane-wave basis set was 360 eV, and the Monkhorst-Pack scheme was used for Brillouin zone sampling [38]. A k-point mesh of $4\times4\times4$ was employed during the GA searches. Much denser k-point meshes (as listed in Table I) were used to refine the structures selected from the GA search in order to determine the ground-state structures. The electronic band structures, density of states (DOS), and Bader charge analysis were also performed for the low-energy structures selected from the GA search [39]. The phonon dispersion spectra were also calculated by the supercell method implemented in Phonopy code [40] using the same exchange and correlation functional as in the total energy calculations and a kinetic energy cutoff of 500 eV.

To investigate the energetic stability of structures at different compositions obtained from GA search, we calculated the formation energy (E_f) of the compound structures using the following definition:

$$E_f(Au_mSi_n) = [E(Au_mSi_n) - m \times E(Au) - n \times E(Si)]/(m+n),$$

TABLE I. The k-point meshes for different compositions.

Atom number	k-point meshes	Compositions
1	16×16×16	Au primitive cell
2	13×13×13	Si primitive cell
4	10×10×10	Au conventional cell, Au_3Si_1, Au_2Si_2, Au_1Si_3
5	9×9×9	Au_4Si_1, Au_3Si_2
6	9×9×9	Au_4Si_2, Au_2Si_4
7	8×8×8	Au_4Si_3
8	8×8×8	Si conventional cell (diamond), Au_7Si_1, Au_6Si_2, Au_5Si_3, Au_4Si_4, Au_3Si_5, Au_2Si_6, Au_1Si_7
10	8×8×8	Au_8Si_2, Au_6Si_4
12	7×7×7	Au_8Si_4, Au_4Si_8
14	7×7×7	Au_8Si_6
16	6×6×6	$Au_{14}Si_2$, $Au_{12}Si_4$, $Au_{10}Si_6$, Au_8Si_8, Au_6Si_{10}, Au_4Si_{12}, Au_2Si_{14}
20	5×5×5	$Au_{16}Si_4$, $Au_{12}Si_8$
24	5×5×5	$Au_{16}Si_8$, Au_8Si_{16}

where m and n stand for the numbers of the Au atom and Si atom, respectively, and E(Au) and E(Si) are the energies (per atom) of the fcc Au and diamond Si crystalline structures, respectively. As listed in Table I, the calculations for the fcc Au and diamond Si structures were also performed with denser k-points, and the calculations gave accurate results for the formation energy using both conventional unit cells and their primitive cells.

III. RESULTS AND DISCUSSES

From the GA search, we found many low-energy crystal structures with similar formation energies. The energies of the lowest energy structures and some of the second best structures we found from all of the 12 compositions were plotted in Fig. 1,

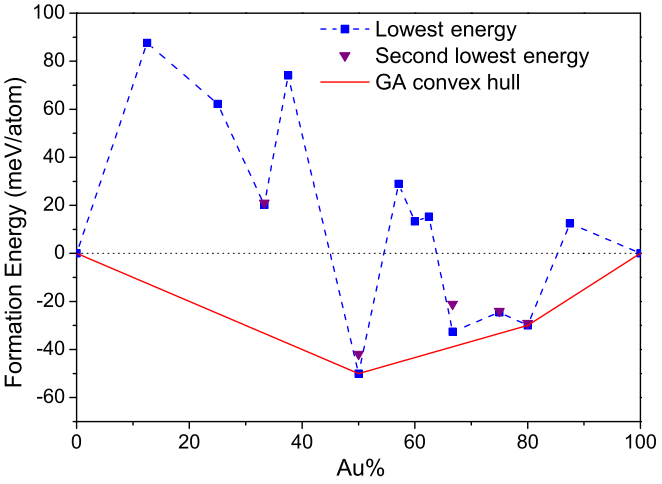

FIG. 1. Formation energies (E_fs) of the predicted Au-Si structures at various Au contents. The blue square and purple triangles represent the lowest energy and the second lowest energy structures, respectively.

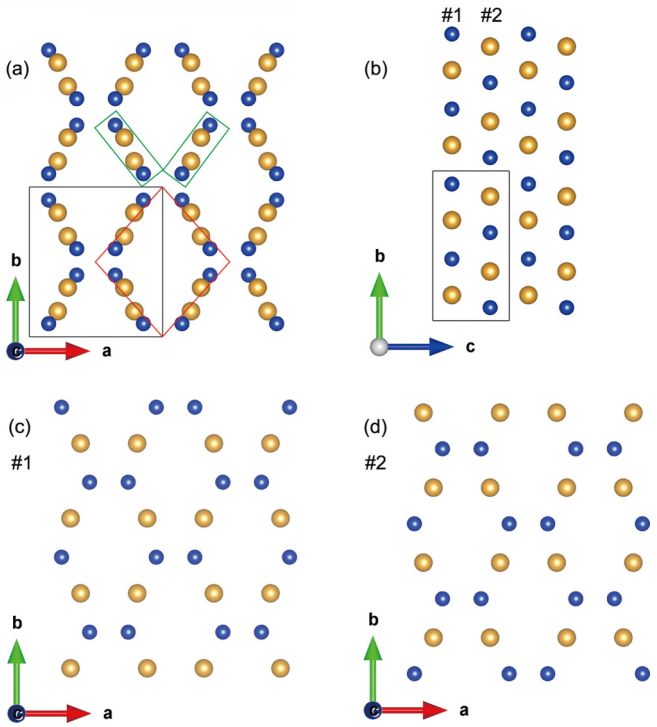

FIG. 2. Lowest energy structure of Au_8Si_8, plotted by VESTA [41]. (a) and (b) Top and side views of the Au_8Si_8 structure; (c) and (d) top view of layer No. 1 and No. 2.

where blue solid squares marked the lowest energy ones and purple triangles represented the second best ones. We noticed that negative formation energies occur at four compositions of 50.0%, 66.7%, 75.0%, and 80.0% Au contents, respectively, indicating that the compounds at these four compositions are stable against segregation into pure Si and Au crystals.

In the papers of Hoshino *et al.* and Tasci *et al.* [20,28], 11 relatively stable Au-Si compounds were predicted, and nine of them were rich in gold, consistent with our convex hull (Fig. 1) in which most of the stable structures are also Au rich. In our prediction, the most stable one is 50.0% of Au content; this also agrees with the results from the literature [13], which suggested that the stable Au-Si alloy should have the Au content around 50.0% to 60.0%.

In the following, we will discuss structures at the four stable compositions in more detail. The structures at other compositions will also be briefly discussed. Some key information about these structures is listed in Table II.

A. Structures of Au-Si = 1:1

The lowest energy structure we found of this composition is Au_8Si_8 (shown in Fig. 2). It belongs to space group of No. 63 *Cmcm*, and its conventional unit cell contains 16 atoms, while it contains eight for its primitive cell. The primitive cell is marked by the red rhombus in Fig. 2(a), and the conventional unit cell is the black rectangle in Figs. 2(a) and 2(b). Compared with Au_8Si_8, another structure Au_4Si_4, as shown in Fig. 3, is of the same composition but relatively higher in energy and belongs to space group No. 59 *Pmmn*. The lattice system of these two structures is orthorhombic.

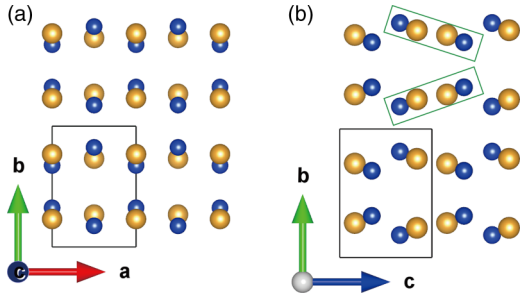

FIG. 3. (a) and (b) Top and side views of the low-energy structure of Au_4Si_4, plotted by VESTA [41].

The lattice parameters of the Au_8Si_8 are $a = 8.275$ Å, $b = 9.317$ Å, $c = 4.751$ Å, $\alpha = \beta = \gamma = 90°$, respectively; its primitive lattice parameters are $a = b = 6.227$ Å, $\alpha = \beta = 90°$, $\gamma = 83.06°$; and two different $8g$ Wyckoff positions are occupied as Au (0.78761, 0.17110, 0.25000) and Si (0.85535, 0.91212, 0.25000), respectively. The lattice parameters of the structure Au_4Si_4 in Fig. 3 are $a = 4.725$ Å, $b = 6.794$ Å, $c = 4.875$ Å, $\alpha = \beta = \gamma = 90°$; the basis Au and Si atoms occupy two different $4e$ Wyckoff positions: Au (0.00000, 0.23143, 0.83688) and Si (0.50000, 0.17532, 0.65236). The formation energy E_f of the structure Au_8Si_8 is -51.11 meV/atom and that of structure Au_4Si_4 is -41.94 meV/atom. Both structures exhibit layer motif, which can be better viewed from the lattice vector **a** in Au_8Si_8 and from the lattice vector **c** in Au_4Si_4. As shown in Fig. 2(a), along the lattice vector **a**, the Au_8Si_8 structure shows an ABAB alternative layered arrangement. The distance between the layers is 2.3754 Å. This structure consists of two types of Si-terminated Au_2Si_2 chains tilted about 41.6° with respect to the direction of the lattice vector **b**, as marked by the green rectangle in Fig. 2(a). These two types of chains form two adjacent zigzag ribbons with a dislocation distance along the direction of the lattice vector **b**. The top view (along vector **c**) of layer A and B were shown in Fig. 2(c) and Fig. 2(d), respectively, and we found that these two layers are rotationally symmetric, in other words, layer A can turn into layer B by rotating 180° along the lattice vector **c**. On the other hand, the atomic arrangement in the structure of Au_4Si_4 is also formed layer by layer; the distance between the layers decreases to 2.3624 Å. The top view was given in Fig. 3(a), and the side view was given in Fig. 3(b). We found Si-terminated Au_2Si_2 chains again as marked in green rectangles. The tilting angle of the chains in this structure is 55.2°, larger than that in the structure of Au_8Si_8.

B. Structures of Au-Si = 4:1

The Au-Si = 4:1 composition system is quite close to the composition of Au-Si eutectic, which is 81% Au content. The two low-energy structures found at this composition are shown in Fig. 4; both have negative formation energies.

The lowest energy structure is I-42m No. 121 Au_8Si_2 [shown in Figs. 4(a) and 4(b)], and it has 10 atoms in a tetragonal cell. This structure type is the same as CI_4, which was reported by Pohl [42]. Its optimized lattice parameters are $a = b = 5.761$ Å, $c = 5.549$ Å, $\alpha = \beta = \gamma = 90°$. The

TABLE II. Optimized low-energy structures of each composition.

Au (%)	E_f(meV/atom)	Crystal system	Space group	Lattice parameter						Wyckoff site
				a	b	c	α	β	γ	
0		cubic	No. 227 Fd-3m	5.4307	5.4307	5.4307	90	90	90	Si:8a
12.5	87.61	tetragonal	No. 115 P-4m2	3.8074	3.8074	11.4187	90	90	90	Au:1b, Si2:2g, Si3:2e, Si4:1c, Si5:2g
25.0	62.21	monoclinic	No. 12 $C2/m$	5.9631	16.1414	5.0383	90	139.88	90	Au:4g Si5:8j Si6:4i
33.3	20.19	monoclinic	No. 12 $C2/m$	7.6706	5.8076	11.0254	90	150.51	90	Au:4i Si:8j
37.5	74.07	triclinic	No. 1 $P1$	4.4432	10.4919	3.8375	88.17	61.91	97.58	1a for all
50.0	−51.11	orthorhombic	No. 63 $Cmcm$	8.2745	9.3170	4.7508	90	90	90	Au:8g Si:8g
50.0	−41.94	orthorhombic	No. 59 $Pmmn$	4.725	6.794	4.875	90	90	90	Au:4e Si:4e
57.1	28.98	monoclinic	No. 8 Cm	5.7586	7.1564	8.5385	90	125.44	90	Au1, Au2:4b Si5, Si6, Si7:2a
60.0	13.35	triclinic	No. 2 P-1	4.6101	9.2177	4.5312	81.65	78.72	86.63	2i for all
62.5	15.31	triclinic	No. 1 $P1$	3.8726	7.2040	5.4341	87.01	87.91	86.52	1a for all
66.7	−32.53	orthorhombic	No. 20 $C222_1$	7.5076	7.2540	9.0930	90	90	90	Au1, Au2:8c, Si:8c
66.7	−21.11	orthorhombic	No. 33 $Pna2_1$	8.400	5.948	4.552	90	90	90	Au1, Au2:4a Si:4a
75.0	−24.50	triclinic	No. 2 P-1	4.7519	6.9668	4.8389	75.56	74.51	79.11	Au1, Au2, Au4:2i Si7:2i
80.0	−29.23	tetragonal	No. 121 I-42m	5.761	5.761	5.549	90	90	90	Au:8i Si:2b
Au (%)	E_f(meV/atom)	Crystal system	Space group	Lattice parameter						Wyckoff site
				a	b	c	α	β	γ	
80.0	−28.02	orthorhombic	No. 20 $C222_1$	7.881	5.977	7.928	90	90	90	Au1, Au2:8c Si:4a
87.5	12.49	monoclinic	No. 8 Cm	8.4497	7.4481	4.9352	90	73.86	90	Au1, Au2:4b Au3, Au5, Au6:2a Si:2a
100		cubic	No. 225 Fm-3m	4.0783	4.0783	4.0783	90	90	90	Au:4a

Au atom at (0.29486, 0.29486, 0.3377) is located at the 8i Wyckoff position, while the Si atom occupies the 2b Wyckoff position Si (0.0, 0.0, 0.5). The structure Au_8Si_2 possesses a rather ordered cross "X" character, shown clearly in its top view in Fig. 4(a). We can see two types of the Au_2Si chain, marked by the green rectangle in Fig. 4(a), tilted about 45° with respect to the direction of the lattice vector **b**. The Si atom marked in a red circle is shared by two types of Au_2Si chains. As shown in Fig. 4(b), the green octagon outlines a basic repeat unit, with eight Au atoms on the edges and with one Si atom located at the center, tilted about 44.4° with respect to the lattice vector **b**. Figures 4(c) and 4(d) shows the second lowest energy structure of this composition. The unit cell of this structure ($Au_{16}Si_4$) is orthorhombic and belongs to the space group $C222_1$ No. 20. The lattice parameters are $a = 7.881$ Å, $b = 5.977$ Å, and $c = 7.928$ Å; the Wyckoff positions of the Au atoms are 8c (0.17959, 0.21212, 0.24212) and 8c (0.50043, 0.27266, 0.07267); and the Si atom is at 4a (0.7264, 0, 0). From Fig. 4(c), it can be seen that the atoms are clearly ordered in an ABCDABCD-stacked multilayer form; each layer contains the same type of atoms. The similar multilayer appearance can be seen from the side view in Fig. 4(d), but the layers are stacked in an ABAB form.

Comparing the I-42m Au_8Si_2 and $C222_1$ $Au_{16}Si_4$ structures with the Au_4Si structure reported by Tasci *et al.* [28], we found that although they have a similar appearance, their space groups are different, i.e., it is p-421c No. 114 for the Au_4Si structure in Ref. [28], while it is I-42m and $C222_1$ for Au_8Si_2 and $Au_{16}Si_4$, respectively, in present work. We also compared their formation energies under the same input parameters and system configurations. The E_fs of the GA predicted Au_8Si_2 (−29.23 meV/atom) and $Au_{16}Si_4$ (−28.02 meV/atom) are lower than −16.68 meV/atom of the Au_4Si in Ref. [28].

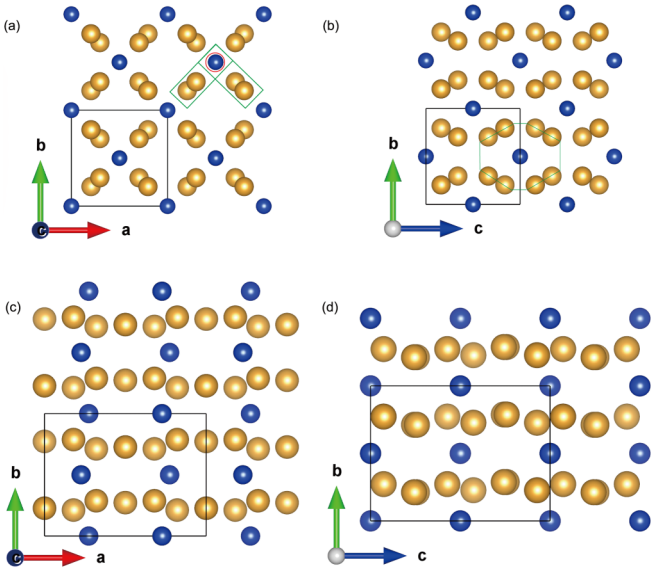

FIG. 4. Low-energy structures of Au_8Si_2 and $Au_{16}Si_4$, plotted by VESTA [41]. (a) and (b) Top and side views of the Au_8Si_2 structure; (c) and (d) top and side views of the $Au_{16}Si_4$ structure.

In addition, we generated their simulated XRD patterns and compared them with experimental XRD images. The major peaks of the $C222_1$ $Au_{16}Si_4$ are close to the experimental data of $Au_{76.7}Si_{23.3}$ [17] but are different when indexed (see the Supplemental Material [43]).

C. Structures of Au-Si = 2:1

Figure 5 shows the structure of $Au_{16}Si_8$, which is the lowest energy structure we found at this composition. The unit cell was drawn by a black rectangle in Fig. 5(a). The cell type is orthorhombic and is of the space group $C222_1$ No. 20.

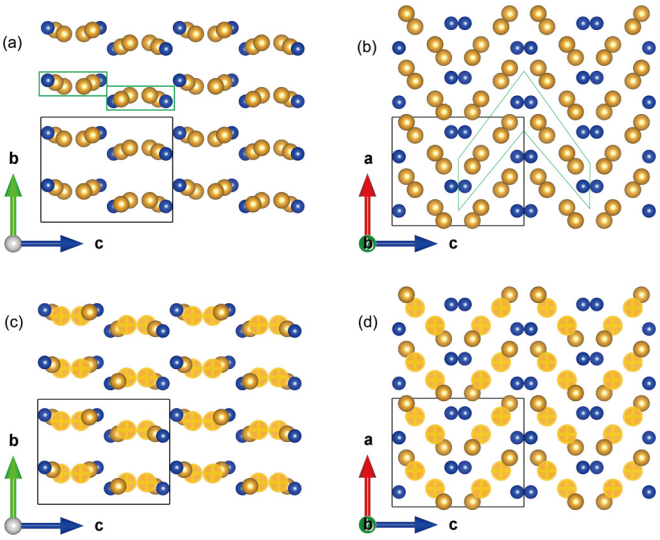

FIG. 5. Lowest energy structure of $Au_{16}Si_8$, plotted by VESTA [41]. (a) and (b) Top and side views of $Au_{16}Si_8$; (c) and (d) top and side views of $Au_{16}Si_8$ with normal Au atoms and cross marked Au atoms, which indicates two different 8*c* Wyckoff positions.

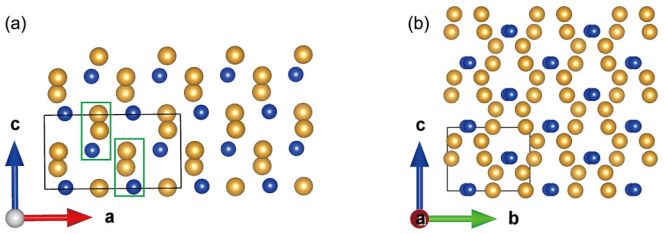

FIG. 6. (a) and (b) Top and side views of the lowest energy structure of Au_8Si_4, plotted by VESTA [41].

The parameters of the unit cell are $a = 7.508$ Å, $b = 7.254$ Å, $c = 9.093$ Å, $\alpha = \beta = \gamma = 90°$, and the atom number is 24. The Au atoms occupy two 8*c* Wyckoff positions: Au1 (0.95211, 0.17066, 0.89139) and Au2 (0.95211, 0.17066, 0.89139); the Si atoms occupy one 8*c* Wyckoff position: Si (0.16823, 0.29256, 0.32582). In addition, the primitive cell of this structure has 12 atoms, and the lattice parameters are $a = b = 5.219$ Å, $c = 9.093$ Å, $\alpha = \beta = 90°$, $\gamma = 88.02°$. The formation energy of this structure is -32.53 meV/atom. The top view of $Au_{16}Si_8$ in Fig. 5(a) shows a layered form. The two types of basic repeat units in a single layer are highlighted within green rectangles. The average distance between each layer is about 3.627 Å. Figure 5(b) is the side view, which presents an ABAB multilayered motif. The layer features, marked in green lines, are connected in zigzag form. The Wyckoff positions of Au1, Au2, and Si were shown in Figs. 5(c) and 5(d), where the Au2 atoms are represented by "+" marked yellow spheres. The nearest distance from Au1 to atom Si is 2.426 Å, and it is 2.536 Å from atom Au2 to atom Si.

The second lowest energy structure at this composition is Au_8Si_4, as shown in Fig. 6. It belongs to the space group $Pna2_1$ No. 33. The unit cell parameters are $a = 8.400$ Å, $b = 5.948$ Å, $c = 4.552$ Å, and $\alpha = \beta = \gamma = 90°$. In this structure, the Au atoms occupy 4*a* Wyckoff positions: Au1 (0.89769, 0.94935, 0.00777) and Au2 (0.90514, 0.41378, 0.78663); the Si atoms occupy one 4*a* Wyckoff position, Si

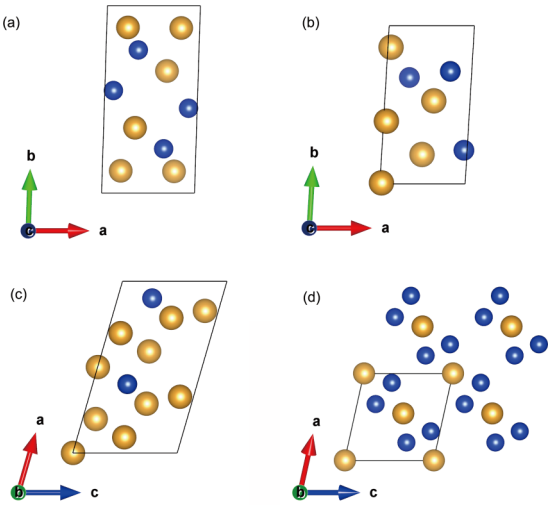

FIG. 7. Lowest energy structures of (a) Au_6Si_4, (b) Au_5Si_3, (c) Au_7Si, and (d) Au_2Si_4, plotted by VESTA [41].

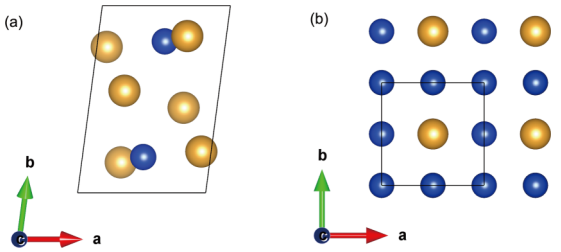

FIG. 8. Lowest energy structures of (a) Au_6Si_2 and (b) $AuSi_7$, plotted by VESTA [41].

(0.15188, 0.22726, 0.01964). The formation energy of this structure is −21.11 meV/atom. Figures 6(a) and 6(b) are the top and side view of the Au_8Si_4 structure. A double layered feature can be seen, and the distance between the layers is about 2.1 Å.

D. Structures of Au-Si = 3:1

In the Au-Si = 3:1 composition (75% of Au content), the result of our search gave a triclinic structure Au_6Si_2 shown in Fig. 8(a). Its unit cell parameters are $a = 4.752$ Å, $b = 6.967$ Å, $c = 4.839$ Å, $\alpha = 75.563°$, $\beta = 74.512°$, and $\gamma = 79.107°$. Its formation energy is −24.50 meV/atom, which is lower than the fcc Au_3Si reported in the paper of Bisit *et al.* [44]. However, the phonon calculation shows that it is not a dynamically stable structure. As we can see from Fig. 1, the E_f is located at the local energy maximum, although it has a negative formation energy. Also, we compared the simulated XRD and experimental XRD image. The main peaks of the Au_6Si_2 are close to the experimental data of Au_3Si [22], but small peaks have deviations (see the Supplemental Material [43]).

E. Structures at other compositions

In Fig. 1, we noticed that the formation energies of Au_2Si_4 (33.3% Au), Au_6Si_4 (60% Au), Au_5Si_3 (62.5% Au), and Au_7Si (87.5% Au) are positive but less than 20 meV/atom above the line connecting the energies of pure Au and Si crystals. These structures might be formed at high temperature or nonequilibrium synthesis conditions. It is therefore worthwhile to briefly discuss the atomic structures of these

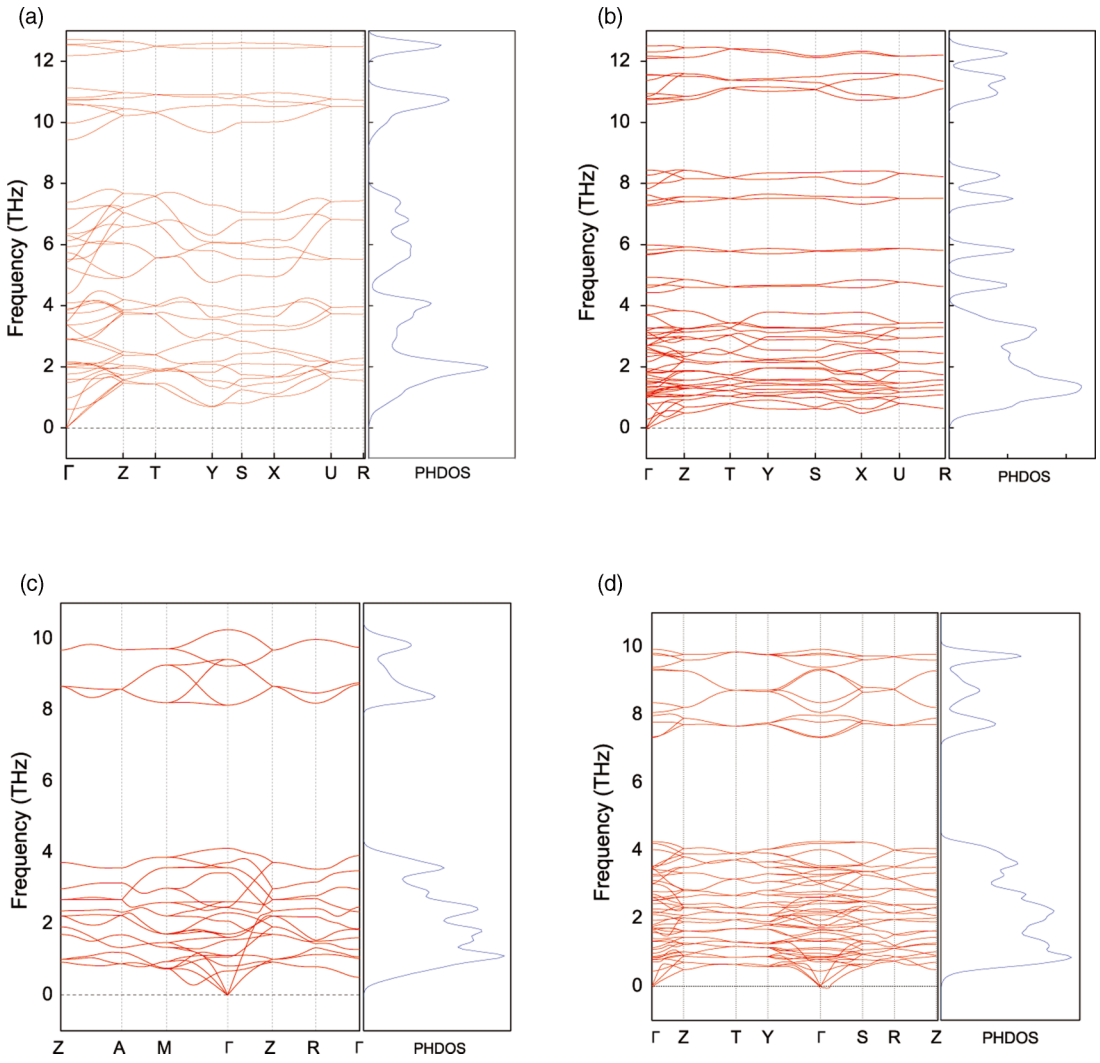

FIG. 9. Phonon band structures of the structures (a) Au_8Si_8, (b) $Au_{16}Si_8$, (c) Au_8Si_2, and (d) $Au_{16}Si_4$.

TABLE III. Bader charges of Au and Si of the Au_8Si_8, $Au_{16}Si_8$, Au_8Si_2, and $Au_{16}Si_4$ structures.

Composition		Au1 ($\|e\|$/atom)	Au2 ($\|e\|$/atom)	of Si ($\|e\|$/atom)
50.00% Au	$Cmcm Au_8Si_8$	−0.684000		0.684000
66.67% Au	$C222_1 Au_{16}Si_8$	−2.120700	−0.276200	2.396950
80.00%Au	I-$42m Au_8Si_2$	−0.186325		0.745400
80.00% Au	$C222_1$ $Au_{16}Si_4$	0.34722	−0.18486	−0.34676

compounds. The lowest energy optimized structures we found from our GA search at these compositions are shown in Figs. 7(a)–7(d).

We note that the structure at the composition 60% Au has the energy located in a local minimum point in our convex hull (Fig. 1). This agrees with the paper of Hoshino *et al.* [20], in which Au_3Si_2 surface crystalline was found on top of the liquid Au-Si alloy. The structure we optimized at this composition is Au_6Si_4 [shown in Fig. 7(a)].

Surface crystalline phases were also reported in the experimental studies at composition 33.3% and 66.7% Au [10,21]. Another study reported that a spherical bulklike crystal structure, which is the first Si-rich Au-Si alloy with 33.3% of the Au content, can be observed after annealing [45]. In our present paper, we found that the energy of the structure at 33.3% Au (i.e., Au_2Si_4) from our GA search is located in a deep minimum in the convex hull (Fig. 1). Although the formation energy of this structure is positive, it is within 20 meV/atom above the line connecting the energies of pure Au and Si crystals. These results are consistent with the experimental observation on the formation of metastable phases at the composition of 33.3% Au [10]. The structure of Au_2Si_4 from our GA search is shown in Fig. 7(d).

Finally, for the 12.5% Au composition, the lowest energy structure $AuSi_7$ obtained from our GA search was shown in Fig. 8(b). This structure belongs to the space group P-$4m2$ No. 115 and contains eight atoms within its tetragonal unit cell. Atomic arrangement of its unit cell is almost the same as diamond silicon.

F. Dynamical stability and electronic structures

Besides the static energetic studies presented above, we performed phonon calculations for the low-energy structures to investigate their dynamical stability. The phonon spectra of 50.0% (Au_8Si_8), 66.7% ($Au_{16}Si_8$), and 80.0% (Au_8Si_2 and $Au_{16}Si_4$) at Au composition were plotted in Fig. 9, showing that structures Au_8Si_8, $Au_{16}Si_8$, Au_8Si_2, and $Au_{16}Si_4$ are dynamically stable without any soft phonon mode. In addition, we have performed elastic constant calculations to investigate the mechanical stability of the predicted structures and found that these four structures meet the mechanical stability criteria [46]. We thus assumed that the $Cmcm Au_8Si_8$, $C222_1$ $Au_{16}Si_8$, I-$42m Au_8Si_2$, and $C222_1$ $Au_{16}Si_4$ could be expected to be energetically, dynamically, and mechanically stable.

We have also investigated the electronic properties of the newly found low-energy structures by performing band structure, DOS, and Bader charge calculations [39]. The Bader charges of Au and Si of four structures were listed in Table III. Negative value indicates excess electron charge with respect to the neutral atom charge. We can see that for most of the structures, except for the structure $C222_1$ $Au_{16}Si_4$, Au presents a negative value while Si presents a positive one, such kind of electron distribution may lead to the particular properties in Au-rich gold silicides. Also, all three of the structures have no band gaps at the Fermi level, around where the DOS is also

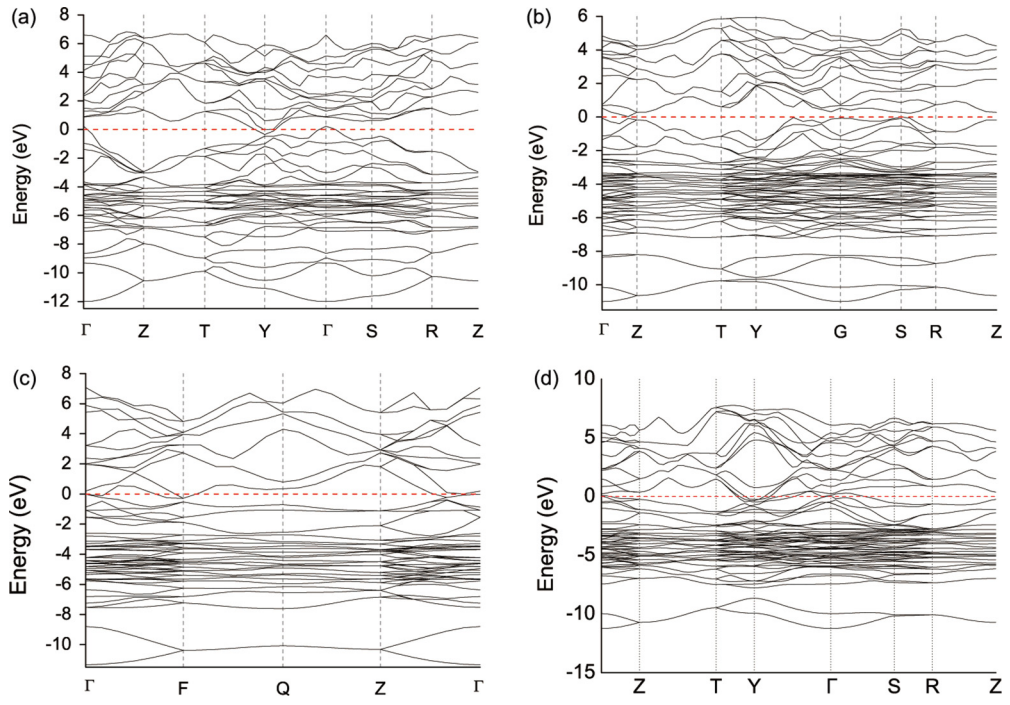

FIG. 10. Electronic band structures of the structures (a) Au_8Si_8, (b) $Au_{16}Si_8$, (c) Au_8Si_2, and (d) $Au_{16}Si_4$.

relatively small (Fig. 10), which is in agreement with that the Au-rich gold silicide may show more metallic properties.

IV. SUMMARY

In summary, we searched for possible Au-Si crystal structures at different compositions and analyzed the tendency of stabilization of different compositions for gold silicide crystals. The calculations were performed by using the GA method combined with DFT calculations. We found that the newly predicted structures Au_8Si_8, $Au_{16}Si_8$, Au_8Si_2, and $Au_{16}Si_4$ are not only energetically stable but also dynamically stable. From our calculations, we noticed that the Si-rich Au-Si compounds may not exist under normal circumstances, and thus the silicon tends to easily segregate out [27] or penetrate to surface [19]. Moreover, the certain stable states may not likely be the compositions with too much gold. In other words, metal-rich phases may also tend to fit to new stable states under certain conditions (chemical, thermal, or physical), and this tendency can even cause the movement of nano-droplets [47]. This may enhance the rationality of our convex hull (Fig. 1), which suggests that the relative stable compositions of Au-Si crystal structures may locate from 50% up to 80% at the Au content and that the per atom formation energy E_f will raise up drastically when Au content is more than 80%.

ACKNOWLEDGMENTS

This paper was supported by the National Natural Science Foundation of China (Grant No. 21273122). This paper was also supported by the U.S. Department of Energy (DOE), Office of Science, Basic Energy Sciences, Materials Science and Engineering Division including a grant of computer time at the National Energy Research Scientific Computing Centre (NERSC) in Berkeley, CA. Ames Laboratory is operated for the U.S. DOE by Iowa State University under Contract No. DE-AC02-07CH11358.

[1] L. Hultman, A. Robertsson, H. T. G. Hentzell, I. Engström, and P. A. Psaras, J. Appl. Phys. **62**, 3647 (1987).
[2] A. K. Green and E. Bauer, J. Appl. Phys. **52**, 5098 (1981).
[3] T. B. Massalski, in *Binary Alloy Phase Diagrams*, 2nd ed. (American Society for Metals International, Materials Park, Ohio, 1990), p. 428.
[4] N. A. Stolwijk, B. Schuster, and J. Hölzl, Appl. Phys. A **33**, 133 (1984).
[5] E. Ö. Sveinbjörnsson, O. Engström, and U. Södervall, J. Appl. Phys. **73**, 7311 (1993).
[6] J. Haubert, N. A. Stolwijkts, L. Tapferll, H. Mehrer, and W. Frank, J. Phys. C: Solid State Phys. **19**, 5817 (1986).
[7] J. S. Lin, C. C. Chen, E. W. G. Diau, and T. F. Liu, J. Mater. Process. Tech. **206**, 425 (2008).
[8] J. B. Hannon, S. Kodambaka, F. M. Ross, and R. M. Tromp, Nature **440**, 69 (2006).
[9] N. Ferralis, R. Maboudian, and C. Carraro, J. Am. Chem. Soc. **130**, 2681 (2008).
[10] O. G. Shpyrko, R. Steitel, V. S. K. Balagurusamy, A. Y. Grigoriev, M. Deutsch, B. M. Ocko, M. Meron, B. Lin, and P. S. Pershan, Science **313**, 77 (2006).
[11] W. Klement, R. H. Willens, and Pol Duwez, Nature **187**, 869 (1960).
[12] D. M. Herlach, P. K. Galenko, and D. Holland-Moritz, *Metastable Solids from Undercooled Melts* (Elsevier, Amsterdam, 2007).
[13] S. H. Lee and G. S. Hwang, J. Chem. Phys. **127**, 224710 (2007).
[14] J. Maddox, Nature **335**, 201 (1988).
[15] S. Kumar, P. K. Sahoo, R. S. Chauhan, D. Kabiraj, U. Tiwari, D. Varma, and D. K. Avasthi, Nucl. Instr. Meth. Phys. Res. B **212**, 238 (2003).
[16] R. Khalfaoui, C. Benazzouz, A. Guittoum, N. Tabet, and S. Tobbeche, Vacuum **81**, 45 (2006).
[17] R. C. Krutenat, J. K. Tien, and D. E. Fornwalt, Metall. Trans. **2**, 1479 (1971).
[18] H. Fujii, S. Tahara, Y. Kato, S. Kohara, M. Itou, Y. Kawakita, and S. I. Takeda, J. Non-Cryst. Solids **353**, 2094 (2007).
[19] A. Hiraki, E. Lugujjo, and J. W. Mayer, J. Appl. Phys. **43**, 3643 (1972).
[20] Y. Hoshino, Y. Kitsudo, M. Iwami, and Y. Kido, Surf. Sci. **602**, 2089 (2008).
[21] O. G. Shpyrko, R. Streitel, V. S. K. Balagurusamy, A. Y. Grigoriev, M. Deutsch, B. M. Ocko, M. Meron, B. Lin, and P. S. Pershan, Phys. Rev. B **76**, 245436 (2007).
[22] G. A. Andersen, J. L. Bestel, A. A. Johnson, and B. Post, Mater. Sci. Eng. **7**, 83 (1971).
[23] X. Zhao, M. C. Nguyen, W. Y. Zhang, C. Z. Wang, M. J. Kramer, D. J. Sellmyer, X. Z. Li, F. Zhang, L. Q. Ke, V. P. Antropov, and K. M. Ho, Phys. Rev. Lett. **112**, 045502 (2014).
[24] B. Meredig and C. Wolverton, Nat. Mater. **12**, 123 (2013).
[25] S. Curtarolo, G. L.W. Hart, M. B. Nardelli, N. Mingo, S. Sanvito, and O. Levy, Nat. Mater. **12**, 191 (2013).
[26] A. Pasturel, E. S. Tasci, M. H. F. Sluiter, and N. Jakse, Phys. Rev. B **81**, 140202 (2010).
[27] S. H. Lee, J. A. Stephens, and G. S. Hwang, J. Phys. Chem. C **114**, 3037 (2010).
[28] E. S. Tasci, M. H. F. Sluiter, A. Pasturel, and P. Villars, Acta Materialia **58**, 449 (2010).
[29] D. M. Deaven and K. M. Ho, Phys. Rev. Lett. **75**, 288 (1995).
[30] M. Ji, K. Umemoto, C. Z. Wang, K. M. Ho, and R. M. Wentzcovitch, Phys. Rev. B **84**, 220105 (2011).
[31] S. Q. Wu, M. Ji, C. Z. Wang, M. C. Nguyen, X. Zhao, K. Umemoto, R. M. Wentzcovitch, and K. M. Ho, J. Phys.: Condens. Matter **26**, 035402 (2014).
[32] M. C. Nguyen, J. H. Choi, X. Zhao, C. Z. Wang, Z. Y. Zhang, and K. M. Ho, Phys. Rev. Lett. **111**, 165502 (2013).
[33] P. E. Blochl, Phys. Rev. B **50**, 17953 (1994).
[34] G. Kresse and D. Joubert, Phys. Rev. B **59**, 1758 (1999).
[35] G. Kresse and J. Furthmüller, Comput. Mater. Sci. **6**, 15 (1996).
[36] G. Kresse and J. Furthmüller, Phys. Rev. B **54**, 11169 (1996).
[37] J. P. Perdew, K. Burke, and M. Ernzerhof, Phys. Rev. Lett. **77**, 3865 (1996).
[38] H. J. Monkhorst and J. D. Pack, Phys. Rev. B **13**, 5188 (1976).
[39] G. Henkelman, A. Arnaldsson, and H. Jónsson, Comput. Mater. Sci. **36**, 354 (2006).

[40] A. Togo and I. Tanaka, Scr. Mater **108**, 1 (2015)
[41] K. Momma and F. Izumi, J. Appl. Crystallogr. **44**, 1272 (2011).
[42] S. Pohl, Z. Kristallog. Cryst. Mater. **159**, 211 (1982).
[43] See Supplemental Material at http://link.aps.org/supplemental/10.1103/PhysRevB.95.134109 for comparison of XRD patterns and information regarding another proposed Au_8Si_2 structure.
[44] O. Bisit, C. Calandra, L. Braicovich, I. Abbati, G. Rossi, I. Lindau, and W. E. Spicer, J. Phys. C: Solid State Phys. **15**, 4707 (1982).
[45] F. H. Baumann and W. Schröter, Phys. Rev. B **43**, 6510 (1991).
[46] J. F. Nye, *Physical Properties of Crystals* (Oxford University Press, Oxford, 1985).
[47] S. Curiotto, F. Leroy, F. Cheynis, and P. Müller, Surf. Sci. **632**, 1 (2015).